Precision Engineering 68 (2021) 174–186

Contents lists available at ScienceDirect

Precision Engineering

journal homepage: http://www.elsevier.com/locate/precision

Current challenges and potential directions towards precision microscale additive manufacturing – Part III: Energy induced deposition and hybrid electrochemical processes

Samira Chizari [a], Lucas A. Shaw [a], Dipankar Behera [b], Nilabh K. Roy [b], Ximeng Zheng [c], Robert M. Panas [d], Jonathan B. Hopkins [a], Shih-Chi Chen [c], Michael A. Cullinan [b,*]

[a] Flexible Research Group, Mechanical and Aerospace Engineering, University of California, Los Angeles, CA, USA
[b] Nanoscale Design and Manufacturing Laboratory, J. Mike Walker Department of Mechanical Engineering, The University of Texas at Austin, Austin, TX, USA
[c] Multiscale Precision Instrumentation Laboratory, Department of Mechanical and Automation Engineering, The Chinese University of Hong Kong, Shatin, Hong Kong
[d] Lawrence Livermore National Laboratory, Livermore, CA, USA

ARTICLE INFO

Keywords:
Microscale additive manufacturing
Focused ion beam
Laser CVD
Meniscus confined electroposition
Electrochemical printing

ABSTRACT

The Part III of the four-part series of articles discusses the challenges and opportunities in microscale additive manufacturing processes, specifically focusing on energy-induced deposition and electrochemical processes. Compared to the direct ink write (DIW) and laser-based processes, the energy-induced deposition methods can fabricate high-resolution, high aspect ratio and complex parts, while the hybrid electrochemical process can be used to fabricate complex parts using a wide range of conductive and photoactive materials. However, the volumetric throughput of these processes is lower than their DIW and laser-based counterparts. The processes that have been explored in this process are Focused-ion Beam Induced Deposition (FIBID), Laser Chemical Vapor Deposition (LCVD), Menicus-confined Electrodeposition (MCED) and Laser-Enabled Electrochemical Printing (LECP). The range of processable materials, feature-size resolution, geometry and volumetric throughput are used as factors to evaluate the current state-of-the-art for these processes. Novel approaches have been proposed in the article to address these challenges associated with microscale AM processes.

1. Introduction

Energy-induced deposition and other hybrid microscale additive manufacturing processes are typically driven by the idea of localized and selective deposition of material through thermochemical and electrochemical means. The primary motivation behind adopting these techniques is the relative maturity and controllability of the vapor deposition and electroplating industries, which allows for the fabrication and selective deposition of thin films critical to high resolution and complex microstructures. In essence, these processes can fall under other major additive manufacturing classes, but we have decided to report them separately because of the significant differences in the resolution, throughput and geometric capabilities of the process. FIBID and LCVD are variants of direct write processes which use gaseous precursors as the starting material and high energy sources such as focused ions or lasers as the selective material deposition mechanism. While these approaches allow for the precise fabrication of complex microparts, the process throughput is limited by the kinetics of the chemical deposition and electrochemical reactions. From an AM perspective, these processes have been used to successfully fabricate 2.5D structures like low aspect-ratio pillars, and 3D parts like helical coils which are discussed in the following sections. This is part III of the series of articles which discuss the potential challenges and opportunities in microscale additive manufacturing processes [1–3].

2. Focused-ion beam induced deposition (FIBID)

2.1. Description of the focused ion beam induced deposition process

Focused Ion beam (FIB) induced deposition or direct write is a 3D process that uses a FIB to selectively deposit materials in precise locations on a substrate. The principles behind FIB induced deposition (FIBID) are largely based on the chemical vapor deposition (CVD) process, and the reactions are similar to those found in laser CVD. The main

* Corresponding author.
E-mail address: michael.cullinan@austin.utexas.edu (M.A. Cullinan).

https://doi.org/10.1016/j.precisioneng.2020.12.013
Received 21 April 2020; Received in revised form 11 December 2020; Accepted 13 December 2020
Available online 15 December 2020

components of a typical FIBID tool include an ion-column, a work chamber with a 6DOF stage, a vacuum system, and a gaseous delivery nozzle system [4]. The ions (typically Ga + due to its low melting point & low corresponding vapor pressure) are generated in the ion-column by the application of a strong electric field on a Liquid Metal Ion Source. The Ga + ion source is the most widely used ion source due to its long-term stability and room temperature operation [5], however there are many other metal ion sources such as Si, Ge, Au, Cr, Bi that have been used in FIBID depending upon the desired application of the tool [6,7]. Plasma ion sources such as Xenon FIBs have also been used for micro-machining applications to achieve a higher throughput [8].

The FIB induced deposition process involves supplying the gaseous precursor to the surface of the substrate with a fine tip nozzle assembly and selectively scanning an ion beam over the gaseous precursor to deposit material onto the substrate with sub-100 nm resolution. As the gases are sprayed they are adsorbed to the substrate and the incoming ion beam decomposes this gaseous precursor into its volatile components (organics), which are desorbed and removed through the vacuum system, and non-organics (metals), which remain on the surface as a thin film [9]. It should be noted that the beam cannot stay at any one location very long else before it starts sputtering away the deposited material. So, the precursor gas needs to be replenished quickly and the beam scanned between the first site and another location further deposition such that damage to the deposited material can be minimized [10]. Another advantage of the process is that it doesn't require the substrate to be flat or rigid, and has been demonstrated on various non-planar surfaces [9]. As a result, the process is also suitable for use on flexible substrates and recently, researchers have demonstrated the deposition of sub 100 nm wide Pt, Co lines on flexible substrates [11]. In fact, FIB induced CVD has been used to create free space wiring 3D nanostructures using carbon [12]. A typical arrangement of a FIBID setup coupled with an insitu imaging tool and some fabricated parts have been show in Fig. 1.

2.2. Materials

2.2.1. Materials capabilities and challenges in FIBID

Focused ion beam deposition can be used with a wide variety of materials including conductors such as Au, Al, Cu, Mo, W, Ta and Pt [14–19], and insulators such as SiOx, TEOS, TMCTS/O2, PMCPS/O2 [20–22]. Because of its maskless deposition capability for both conductors and insulators, it has been widely used in semiconductor manufacturing for low volume repair work, mask repair, device modification, and IC debugging, as well as in applications such as micro-sensor/micro-actuator fabrication [23,24], optical metamaterials [25] and development of micro-nano 3D structures [10,26,27]. Although the foundation of ion physics and ion emission science was developed in academic research, the machine development effort was continued only by a few companies geared towards the needs of IC industry-their primary market which is evident from the list of commonly deposited materials above. However, other efforts have been carried out by the researchers in deposition of various materials for different applications. Matsui et al. developed many functional micro/nano structures using FIB-CVD including 3D nanorotors using Phenanthrene ($C_{14}H_{10}$), biomimetic structures and bio-nano tools for cell organelles manipulation, nanoactuators with coil structures, and neural interfaces connecting human nervous system to external devices using diamond like carbon [24,28–30].

The deposition of a material using FIB is limited by the availability of volatile organic or inorganic compounds of the desired material. In principle, all precursors used in CVD can be used for FIBID, materials including precursors for depositing metals, metalloids (binary metals), ceramics [31] and carbon. Metal organic precursors such as metal carbonyls and organometallics are quite popular as the precursor materials for deposition of the corresponding metal. In terms of purity of deposited metal, metal carbonyls result in better deposition compared to

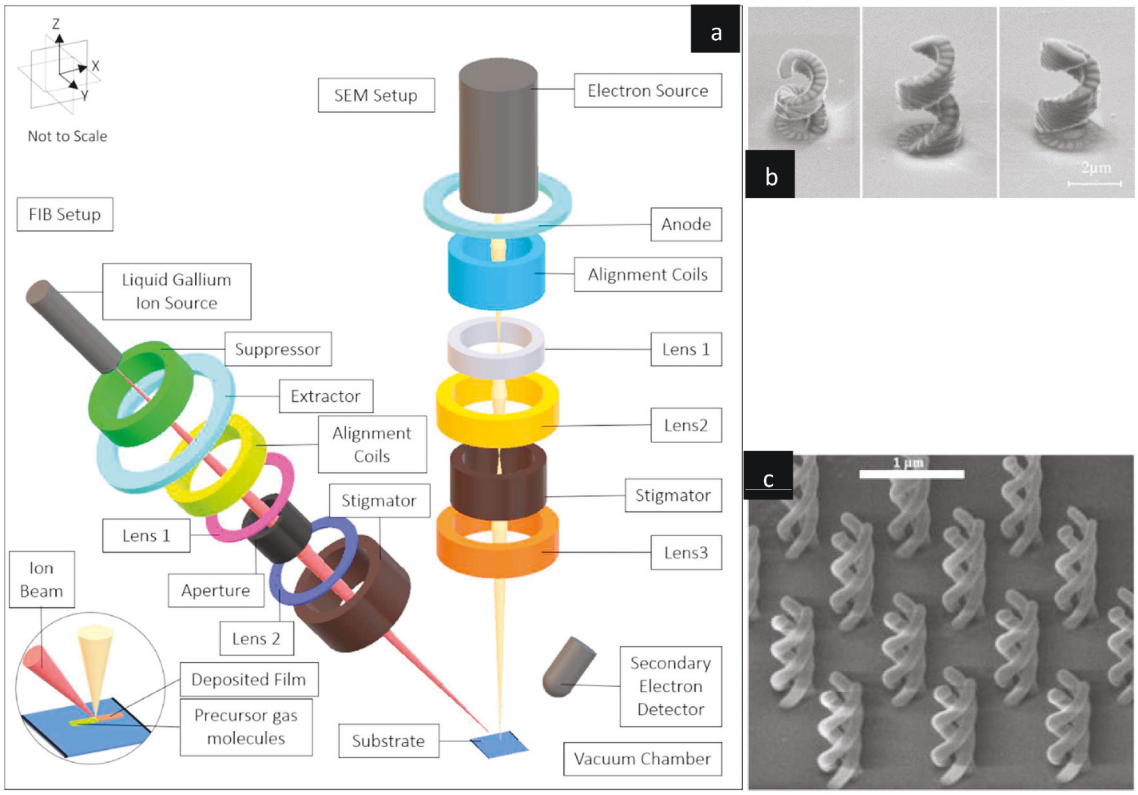

Fig. 1. (a) Schematic of a dual-beam (FIB + SEM) setup for in-situ monitoring of FIBID fabricated 3D parts (b) FIB induced nanostructures [9] with overhangs. (c) Triple-helical nanowires fabricated using FIBID process for photonic applications [13] (Reproduced with permission from Ref. [13]. Copyright Nature Publishing Group.).

organometallics, however the toxicity of metal carbonyls is much higher than organometallics [7]. Metal halides are also used for their high purity, but they are also highly toxic and corrosive [32]. The research needed to identify suitable precursors to achieve high purity of deposited materials with desirable properties is, on the whole, still lacking for materials not used primarily in the IC industry. An extensive list of the different categories of precursor materials has been compiled and reviewed by Utke et al. [7]. Another drawback of current metal ion source based processes lies in the problem of substrate contamination with elements from corresponding ions, elements from the precursor gases causing a degradation in mechanical, thermal, optical and electrical properties of the part [21,33].

2.2.2. Possible approaches to overcome material challenges in FIBID

Selecting appropriate precursor material such that it decomposes more rapidly than it can be sputtered away, is critical for the successful deposition of the desired material. An ideal precursor should stick and stay on the substrate for long durations until it is ready to be dissociated for deposition. The volatile compound and non-desired constituents formed during the irradiation of precursors should desorb readily. Since, both the ligands and the material to be deposited originate from the same parent molecule and have opposing requirements, finding suitable precursors with high purity of the deposited material is challenging. Although many precursors have been identified for the commonly used metals for deposition, more research is required to identify the ideal precursors for other materials, and to understand the precursor dynamics, including their irradiation chemistry, the role of surface kinetics, diffusion, adsorption/desorption from the substrate, and the effect of substrate properties/temperature. Additionally, to improve the purity of the deposited material and reduce contamination from the ion source, using lighter elements as ion sources such as He + or Ne + could lead to lower ionic contamination which is significant with heavier element ion sources [34].

2.3. 3D feature fabrication

2.3.1. 3D feature fabrication capabilities and challenges in FIBID

One of the main benefits of this process is that it can be employed for fabrication of highly complex geometries & shapes with resolutions better than 100 nm [12,35,36]. Among the many micro and nanoscale processes, FIBID has the capability to produce structures with one of the widest ranges of intricate designs. The process also enables deposition of complex 3D shapes with overhanging features. This ability to fabricate overhanging features enables the process to be used for hermetic encapsulation of micro-sensors [37]. However, the fabrication of intricate structures including overhangs requires a precise control of the growth rate and growth direction, and thus good control over the process parameters such as gas flow rate and direction is highly desired. For depositing complex shapes, a tradeoff exists between the accuracy/cleanliness of features and processing time. A fine beam (small ion current) and small overlap between consecutive layers can provide a fine resolution overhang with little debris while if a high deposition rate is desired, a higher current beam is needed which can lead to coarse features and debris under the fabricated overhang.

2.3.2. Possible approaches to overcome 3D feature fabrication challenges in FIBID

The size and complexity of parts that can be deposited with FIBID is limited in practice by the processing time available. Complex structures up to 10s of microns can be typically fabricated in a reasonable amount of time. However, as the complexity of parts increases, the control of process parameters such as growth angle and growth direction grows in importance in order to be able to maintain part geometry at high resolution [38]. Robust models of the process must be developed and simulated offline to achieve a high fidelity simulation and process parameter optimization for complex three dimensional geometries [39]. As the models and process mature, and the processes are guided more and more by the simulations and model predictive control, the speed of the process can be improved while fabricating intricate geometries and structures with different materials.

2.4. Feature size resolution

2.4.1. Feature size resolution capabilities and challenges in FIBID

The process can deposit layers as thin as 10 nm [7] with minimum lateral feature resolution on the order of tens of nanometers (10–100 nm) and aspect ratios of 5–10 [10,40]. The minimum feature size is limited by the FIB spot size on the substrate. This spot diameter has a direct relationship with both the current density and the ion beam current. However, the interaction volume of the beam with substrate can be significantly higher due to a large number of cascaded collisions of heavy metal ions (such as Ga+) with the substrate as the ions penetrate the substrate, thus degrading the achievable resolution [34] at the surface. The process requires a tight control of beam parameters such as dwell time, refresh time, focus, and beam spacing for realizing high resolution features.

2.4.2. Possible approaches to overcome current limits in feature size resolution for FIBID

Since the minimum feature resolution is dependent upon the interaction volume, it is imperative to shrink the interaction volume to improve the feature resolution. Writing into free space eliminates the substrate contribution to interaction volume and consequently, finer resolutions can be achieved. The push for finer resolution has led to the development of FIB tools with lighter elements ion sources such as He+ and Ne+ [41,42] with theoretical resolutions of sub-1nm and 1 nm respectively. These lighter elements penetrate further and come to rest deeper in the substrate and have fewer collision cascades at the surface leading to a smaller interaction volume and hence, sharper feature resolution [43]. Depositing sub-10 nm resolution features requires a strict control and optimization of beam profile and minimizing the lateral energy spread of the beam. Recently, some articles have reported He+/Ne + induced deposition results with lateral resolutions as small as 10 nm as well [26,44,45]. Since the resolutions in single digit nm have already been demonstrated, there is only a small window for further improvement to move closer to the theoretical resolution of features that can be deposited with FIB.

2.5. Throughput

2.5.1. Throughput capabilities and challenges in FIBID

Although FIB has benefits such as generation of 3D structure with high complexities and resolutions smaller than 100 nm, the size of the structures that can be obtained by FIB is severely limited by processing speed. FIB is slower than both laser induced chemical vapor deposition and micro-stereolithography, however the achievable resolution is much better. As the resolution of the process is so small, its deposition speed or volumetric throughput, consequently, is limited. Thus, making larger structures (>100 μm) can be extremely time-consuming [10]. The volumetric throughput of the FIBID process is generally 0.05–0.1 $\mu m^3/s$ [9,46]. This makes FIB very limited for scaling and high throughput applications, and the primary reason why it has traditionally been only used for repairs or other low throughput tasks. With finer resolution, this throughput falls even further. For higher deposition rates, a higher ion current can be used, however, the features are expected to become coarser, degrading the resolutions achievable [9].

2.5.2. Possible approaches to overcome throughput challenges in FIBID

High process throughput is a critical requirement for scalability to a production environment. To improve the throughput of the FIBID process, a mask-based solution along with a collimated wide ion beam was developed called ion projection lithography (IPL). In IPL, ions are

extracted from a lighter element ion source ($H+$,H_2+, H_3+, $He+$) and collimated through a mask with the imaging pattern, after which they are accelerated through a set of electrostatic lenses that project the ions onto a wafer substrate, where the ions penetrate and modify the substrate materials [47,48]. The process was largely considered as one of the promising NGL (next generation lithography) techniques in early 2000s, however due to implementation difficulties and low throughputs, it was never widely adopted in industry.

Another offshoot of projection-based lithography that uses a multi-beam solution has been tested and developed. The process does not use a stencil mask and is termed projection mask less patterning or multi-beam ion lithography. The technology uses thousands of tiny beamlets generated through a programmable aperture mask. The mask is de-magnified by a 100–200X factor and hence, the mask opening of 3.5um can be patterned at 35 nm to 17.5 nm resolution spots on the sample [49]. This technology has received more positive response and has been favorably adopted to reduce the costs of mask writing for lithography tools [7,50,51]. Another potential solution to the throughput problem could be to design and develop a process which uses a variable beam size and shape so that a fine beam can be used for deposition of high resolution features and the beam size can be made larger for coarser features where higher throughput is desired. This kind of solution has been researched and implemented for other processes [52] such as variable shaped electron beam lithography [53].

2.6. Prognoses

Focused ion beam induced deposition provides a solution for high resolution, sub-μm additive manufacturing of several metals and insulators typically used in semiconductor industry. However, many technical challenges remain in its adoption and implementation as a complete additive manufacturing solution in a higher volume production environment. There is significant scope for improvement in terms of identifying precursors for depositing different materials including ceramics, polymer-based low-K dielectrics, and developing robust process models for a highly reliable process for micro-nano AM. With the current throughput levels, the process is best suited for prototyping and manufacturing of high precision micro and nano devices with a wide variety of materials in addition to its applications in IC industry. For successful adoption in high volume manufacturing environments, the process can be integrated with macroscale AM processes so as to achieve fine resolution in critical regions of a part combined with a high throughput in less critical regions.

3. Laser Chemical Vapor Deposition (LCVD)

3.1. Description of the LCVD process

Laser chemical vapor deposition (LCVD) is a method for selective deposition of solid materials via localized chemical reaction driven by a focused laser beam. The LCVD approach can be used to create large-area (mm^2 scale) films [54] or true-3D microstructures out of a wide variety of both conductive [55] and non-conductive materials [56]. LCVD has several advantages over traditional chemical vapor deposition (CVD) processes (*e.g.*, low-pressure CVD, metal-organic CVD, or plasma-enhanced CVD) including increased deposition rate [57], decreased process temperatures [58], superior spatial resolution [59], and the ability to produce true-3D microstructures with micron or submicron-sized features [60], including periodic structures [60]. The LCVD approach works with almost all of the materials that can be deposited by traditional CVD [61], and has been used to deposit materials with improved mechanical properties and thermal stability [59]. The LCVD approach is compatible with various process monitoring techniques that improve uniformity and consistency including optical interferometry [62], spectroscopy (optical radiation monitoring) [58], pyrometry (thermal radiation monitoring) [63], and CCD-based image acquisition [58]. Fig. 2 shows a typical schematic of the LCVD process and some parts made using the process.

LCVD processes are generally categorized as either pyrolytic [64] or photolytic [65] depending on the type of mechanism which initiates the chemical reaction. Pyrolytic LCVD processes are thermally-driven reactions in which a focused laser beam is used to locally heat the surface of the substrate to the temperature required for decomposition of the adjacent gaseous precursor, resulting in deposition of solid material. The pyrolytic LCVD approach is often used to deposit small regions of 2D films faster than traditional CVD processes due to its faster localized heating and cooling rates [66]. In contrast, photolytic LCVD processes use photons from focused laser beams to directly dissociate reactant gases, resulting in precise deposition of solid material in either 2D films or 3D structures. Photolytic LCVD systems typically utilize pulsed lasers as their high peak power levels more effectively drive the chemical reactions [54]. One limitation of this approach is the need to closely match the laser wavelength with the absorption spectrum of the reactants [61]. However, the main advantages of this reaction is that it can more readily add material in 3D configurations, and it occurs at lower temperatures than pyrolytic processes, thus inducing less thermal stress builds up in the resulting structures [61].

3.2. Materials

3.2.1. Materials capabilities and challenges in LCVD

LCVD has been used for fabrication of fibers with a variety of materials that have been traditionally used in CVD [61]. This includes carbon nanotubes [63], silica [62], tungsten [56,60], diamond-like carbon [56], aluminum [55], aluminum oxide [69], iron oxide [54], silicon carbide [66], boron [66], boron nitride [66], molybdenum [66], nickel [59], titania [59], Yttrium oxide [70] and titanium carbide [59]. LCVD is limited by the development of precursor chemistries. This limitation is shared by conventional CVD, and the range of available materials is slowly expanding as increased research interest in microfabrication drives greater material variety.

3.2.2. Possible approaches to overcome materials challenges for LCVD

Increased research and development in the CVD precursor material variety will slowly expand the material space available to LCVD. The limitations on precursor development are mainly centered around engineering the thermodynamics of the chemistries. This presents unique challenges for each target chemistry. LCVD offers an opportunity to overcome some present challenges with material deposition via wavelength targeted interaction with the deposited materials. For instance, specific wavelength absorption during the material deposition could be used to aid in breaking the oxygen bond to push towards pure metal deposition. Metals are typically difficult to deposit due to their propensity to oxidize, but a wavelength specific laser may be able to drive reaction kinetics towards a more favorable space. Such a system may use one laser for photolytic or pyrolytic deposition and a second to drive the reaction kinetics.

3.3. 3D feature fabrication

3.3.1. Capabilities and challenges in LCVD for fabricating 3D features

3D structures can be fabricated in LCVD by coordinated movement of laser spot with respect to the substrate. Lehmann and Stuke reported fabrication of a laser driven micro-motor [71], three-dimensional aluminum grid structure [72], and a micro-cage made out of aluminum oxide with rods of diameter 5–20 μm[69] (Fig. 2b). Stuke et al. later demonstrated usage of micro-cages for trapping and handling of polarizable particles [55]. The most common structure for the present state-of-the-art in LCVD is a thin wire [55,57], however other features have been generated [61] including dots and in-plane lines [60]. These structures are created by extruding the reaction point of the system through space. Complex non-wire 3D structures place changing

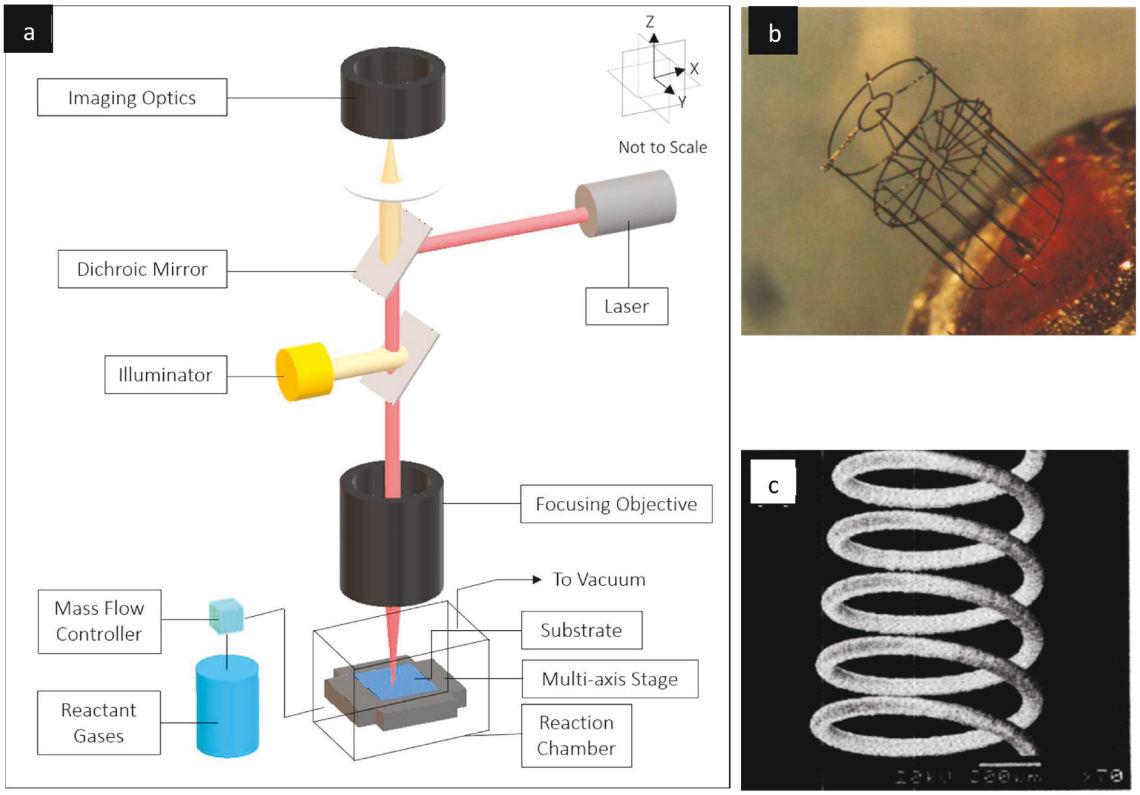

Fig. 2. (a) Schematic of a typical LCVD system setup. Continuous or pulsed laser is used to pyrolytically or photolytically drive chemical reactions that decompose gaseous precursor and deposit solid material. (b) Freestanding aluminum oxide microstructure, diameter of the rods is about 20 μm (photo reprinted taken from Ref. [67] (c) Tungsten carbide microsolenoid (photo reprinted taken from Ref. [68]).

demands on the reaction kinetics when approached as a conventional layer-by-layer print approach, and as such LCVD research has focused on wires.

Pyrolytic processes utilize the nonlinear thermal breakdown threshold to localize the decomposition operation at the point of laser focus. This avoids unwanted reactions outside of the target zone. Pyrolytic processes must be initiated on an absorbing surface which transfers optical energy to thermal energy. This can be on the substrate or a section of the built structure. The pyrolytic process, therefore, requires careful planning to determine the optimal build order. Pointwise operation with no cured material above it leads to the best fabrication quality, which can limit the kinds of structures produced. Any material above the build point is likely to be heated by the beam and may suffer thermal damage or unwanted material buildup. Reaction kinetics (powers, rates, gas pressures) tuned around pointwise diffusion kinetics may prove difficult to implement in more complex geometrics. The process could continue to rely on a pointwise raster scan deposition; however it would face similar challenges as found in metal AM sintering with thermal management [73,74].

Photolytic processes, being less dependent on a nonlinear threshold, are less selective in the location of the reaction, meaning that a slight decomposition operation may occur outside of the focal point making it difficult to produce 3D structures using this method.

3.3.2. *Possible approaches to overcome 3D feature fabrication challenges in LCVD*

A path to expanding the feature geometry capabilities of LCVD would require modification of the nonlinear thresholds governing the deposition reaction to make these thresholds more amenable to proximity with a partially created structure. This is likely to be difficult with the pyrolytic process, as thermal diffusion is difficult to control. The photolytic process offers an opportunity via the transfer of recent advances in laser driven AM processes [75–77]including two-photon (TPP) interactions [69] which are now much more widely available. Two-photon reactions occur via transfer of the combined energy of two photons and are localized to the focal point of a (typically) pulsed which locally reaches sufficient photon flux to drive the reaction [76]. A TPP photolytic LCVD process could localize the decomposition to a single build point in space and could thus print within complex existing structures without depositing material elsewhere through the structure. The development of the TPP compatible precursor would, however, pose a significant research hurdle.

3.4. *Feature size resolution*

3.4.1. *Feature size resolution capabilities and challenges for LCVD*

The minimum fabricated feature size in this process is dependent on the wavelength of the laser used (i.e. minimum spot size based on diffraction limit), energy density at the deposition zone, and thermal behavior of the substrate. Film thicknesses of less than 100 Å and up to 20 μm have been reported [59]. Williams et al. provided a deposition layer thickness ($h(v_s, t)$) estimation equation for diffusion-limited reactions, in which ω_0 is the laser spot radius, R_0 is the axial growth rate, $v_s$is the scanning speed, and t is process time [78]:

$$h(v_s, t) = \frac{\sqrt{\pi}\omega_0 R_0 t}{\sqrt{\pi}\omega_0 + 2(v_s t)} \tag{12.4}$$

A typical printing spot size of a few μm has been reported [64], but the ranges cover from sub-micron [60] to 5 μm [56] up to around 20 μm [55]. The limits on feature size are driven by the build spot size, which is in turn limited by the control of the nonlinear reaction threshold physics. Pyrolytic processes are limited by the control of the thermal profile via a combination of laser focus and heat dissipation mechanisms as main factors. Photolytic processes are limited by the laser focus as a

main factor.

3.4.2. Possible approaches to overcome current limits in feature size resolution for LCVD

The pyrolytic approach is unlikely to offer any significant room for feature size improvement, given the difficulty in engineering a precise thermal profile. Photolysis may offer more space for improvement. The use of the two-photon reaction offers a means to significantly reduce the reaction zone below the diffraction limited size of the laser focal point. While the reaction kinetics and mobility of the gas may alter the results of the TPP process, it is unlikely to provide a reduction in the size of the reaction spot.

3.5. Throughput

3.5.1. Throughput capabilities and challenges for LCVD

Generally, deposition rates reported for LCVD are increased with higher pressure of gases, increased laser power and power density, and increased scanning rates [79]. Higher process temperatures also accelerate the growth rate exponentially based on chemical kinetics, however the rate will be ultimately limited by the mass transfer and diffusion of gases at the deposition zone [61,67]; which can be idealized as a point in free space with no rate limiting constraints around it. The reported deposition rates for fibers with average diameter of around 10 μm are in the order of 0.5–5 mm/s (0.14–1.4 mm^3/h), with extremes up to 12 cm/s[56] (34 mm^3/h). Williams et al. reported fabrication of freestanding coils (Fig. 2c) with deposition rate as high as 3.5 mm/s for carbon and 175 $\mu m/s$ for tungsten-carbide [78]. Banal et al. reported wide area (15 mm spot size) surface growth at rates up to 300 mm/h (≈50 mm^3/h) scaling with applied laser power up to 250W at which point the deposition rates were likely enhanced by laser-generated plasma at the solid-gas interface [70]. With these relatively low throughputs, LCVD has not been considered a promising method for bulk production, but with current progress in holographic beam-splitting, this deposition technique has the potential to be parallelized to yield higher volumetric rates [68]. Higher deposition rates will likely be governed by the details of high-energy laser-matter interactions as indicated in Refs. [70] via the plasma enhanced deposition rates. Such effects could be modulated by choice of pulse wavelength, intensity and temporal shape to meet the specific users' objectives.

3.5.2. Possible approaches to overcome current throughput limits in LCVD

The LCVD process is amenable to a parallelization of the build spot. Each spot interacts with a small volume of space, drawing down the precursor species in this space through the consumption at the reaction point. Outside of a characteristic distance, the gas species concentration increases to the overall average value. Such diffusion behavior allows point-wise build operations to occur at much higher rates than standard planar CVD 1D diffusion operations [56]. It may be possible to successfully parallelize the process if additional points are operated in the part volume and are constrained to stay several characteristic distances apart from one another.

The fundamental limits to build rate parallelization may be envisioned as a part material build rate per volume of gas. A single point in space can only pull in material from the gaseous environment so fast and has a rough boundary of effect. Outside of this boundary, gas species are not drawn down significantly. Attempting to build faster than this will simply deplete the local area of the chemical species needed for the reaction, leading to diminishing returns in close packed parallelization. Overcoming printing rate will require careful attention to control of parallelized build points with handling that manages for the depletion zone around each build point. It will also likely require careful modulation of the light pulse via wavelength, intensity, and temporal shape to ensure the high-energy laser-matter interactions are tightly controlled.

3.6. Prognoses

The LCVD process can fabricate highly complex true-3D structures. However, metals are difficult to deposit since they are more susceptible to oxidation. A possible solution for that would be to use multiple laser wavelengths to tune the deposition process and improve the reaction kinetics. While this process has been primarily used to demonstrate wire-like structures, layer-by-layer 3D structures have been less explored using this process due to challenges with the reaction kinetics. There is a lot of potential to improve the throughput of the process by parallelizing the build spot. However, the rate at which precursor material is drawn within a volume remains a fundamental limitation to a parallelized LCVD process.

4. Meniscus confined electrodeposition (MCED) process

4.1. Description of the MCED process

The concept of electrodeposition has existed for several centuries, mainly used for surface modification and improving corrosion resistance of metals. The idea of extending it to microscale AM fabrication was primarily driven by the need to develop novel methods for creating metallic wire bonds and chip-scale interconnects [80,81]. The potential advantages of an electrochemical additive manufacturing technique like this include fabrication of freestanding, pure metal structures, which do not need further post-processing. There are two main approaches to achieve a meniscus-confined electrodeposition regime. First, with novel use of micro/nano-pipettes, the electrodeposition process can be localized to a specific point on the substrate. The pipette containing metal salt solution and an electrode (anode) is moved towards the substrate (cathode) until a liquid meniscus is established between them. When an electric potential is applied across the substrate, the metal ions in the pipette undergo reduction, resulting in confined metal electroplating within the volumetric element. The second approach uses a microelectrode in a metal bath solution, which acts as the anode. Local electrodeposition occurs between the microelectrode and the substrate when an appropriate electric field is introduced across them [82]. The 3D structure forms with a conventionally cylindrical cross section with the meniscus defined by a nozzle with circular cross section. This makes the process lucrative for applications in wire bonding and freestanding pillar-like structures with specific applications in microelectronics. The growth of the 3D structure is defined by the rate of electrochemical reduction. The key physical mechanisms involved in ionic transport between the anode and cathode are convection, diffusion and electromigration [80,83,84]. The ability of this process to achieve microstructures without additional annealing/sintering steps, with a resistivity of ~1.8 times of the bulk metal makes it critical for several potential microscale AM applications [85]. The MCED process and fabricated parts are shown in Fig. 3.

4.2. Materials

4.2.1. Materials capabilities and challenges in meniscus-confined electrodeposition

The process has been repeatably used to fabricate 2.5D structures of Cu, Pt [80,85] and 2D line patterns of Ag [87]. However, the range of materials that can be printed is very narrow. The key requirement of the material is that a viable electrochemical reduction step can be initiated, and, therefore, a conducting medium and substrate is required. An advantage of this process is the independence to material size and morphology, unlike some other microscale AM process which must employ nanoscale particles for achieving the required resolution. Since the process is limited to a conductive substrate, the process is not yet suitable for flexible electronics applications which use compliant ultrathin glasses and plastic films.

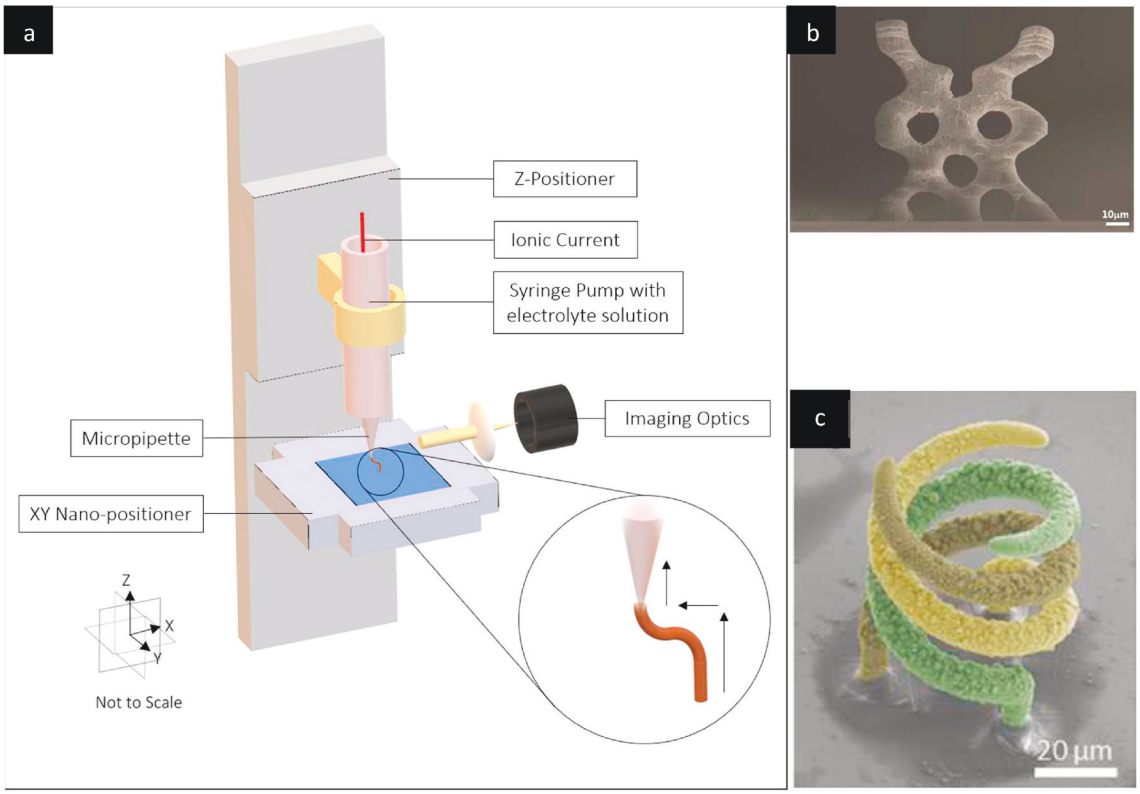

Fig. 3. (a) Schematic of a typical MCED system setup. There are two primary approaches to initiate electrodeposition of metals. The first one involves establishing a meniscus between the micropipette and the substrate and when an electric potential is applied across the substrate, the electrodeposition of metal occurs within the meniscus. The other approach uses a microelectrode dipped in a metal salt solution bath and acts as the anode. It induces local electrodeposition when an electric potential is applied across the microelectrode and the substrate (cathode)(b) (scale bar = 10 μm) Scanning electron micrograph of a electrodeposition based 3D freestanding Cu mesh architecture [86] (Reproduced with permission from Ref. [86]. Copyright John Wiley & Sons, Inc.). (c) A triple helical structure fabricated using a maskless MCED process with force-controlled nanopipette for accurate position control [82] (Reproduced with permission from Ref. [82]. Copyright John Wiley & Sons, Inc.).

4.2.2. Possible approaches to overcome materials challenges for MCED

Electrodeposition of 2.5D and 3D structures using conductive polymer nanostructures like polyaniline (PANI) [88] and polypyrrole (PPy) [89] may be possible. Other conductive polymers can also be exploited using this process including poly(3,4-ethylenedioxythiophene)-poly-(styrene sulfonate) (PEDOT:PSS). Kim et al. [88] demonstrated the polymer nanowire array fabrication by leveraging oxidative polymerization of pyrrole in air and guided by the growth of the meniscus.

4.3. 3D feature fabrication

4.3.1. Capabilities and challenges for fabricating 3D features using MCED

Freestanding 2.5D pillar-like and wired structures have been fabricated using the Meniscus-confined electrodeposition process [80,82]. The primarily applications for the MCED include wire bonds and interconnects for microelectronics applications. Overhanging structures with angled features do not need support structures [81]. However, like DIW, there are challenges associated with fabricating repetitive structures as the process is more suited for continuous fabrication of wire-like structures. The key problems with transitioning from continuous wire-like structures to true-3D repeatable microproducts are associated with the difficulty getting menisci on demand at desired positions [82,90]. The stability of the meniscus depends on the humidity, substrate wetting properties and retraction speed [80,85]. If the speed of nozzle retraction is faster than the growth of the reduced metal structure, there is a possibility of pattern discontinuity and re-establishing the meniscus can be difficult.

4.3.2. Possible approaches to overcome 3D feature fabrication challenges for MCED

A commonly used approach to fabricate complex spiral and overhanging structures is using custom shaped pipettes that can encompass a wide range of designs. Hu and Yu [81] used FIB milling to design micro/nanopipettes which can fabricate complex 3D structures. Hirt et al. [82] used cantilevered probes used in atomic force microscopy (AFM) with a micro-channeled aperture to deposit the fluid and initiate local reduction of metal ions under the tip. In their FluidFM process, once the desired height of the structures are reached, the deflection of tip acts as a feedback loop to change the position of electrodeposition and fabricate continuous structures. A similar approach was employed by Momotenko et al. [91] in a process called scanning ion conductance microscopy (SICM). They used a dual nozzle pipette design, where one of the channels consists of the metal salt solution and the other is used as a feedback by measuring the ionic flux using electromigration. It is important to note that both the processes take place in a supporting electrolytic bath, and therefore the problems associated with the establishment of the liquid meniscus can be bypassed. There are, however, trade-offs between the minimum feature size resolution and throughput that can be achieved using both FluidFM and SICM.

4.4. Feature size resolution

4.4.1. Feature size resolution capabilities and challenges in MCED

In the absence of any externally applied force on the liquid meniscus, the minimum reported feature size that can be laterally deposited depends on the geometry and size of the nozzle. However, solvent evaporation from the free surface of the meniscus can lead to wire diameters

as small as half of the exit nozzle diameter. The highest reported resolution for MCED of vertical metal wires is around 100 nm[81] and for conductive polymers is around 50 nm[89]. It must be understood that the theoretical resolution can be potentially much smaller, depending on the size of the nanopipette, but there are several practical disadvantages including nozzle clogging, high applied pressures, and extremely low throughputs [80–82]. The meniscus size also depends on the wetting properties of the substrate, air humidity, and nozzle speed. The uniformity of meniscus growth depends on the thermodynamic stability of the metal, air, liquid meniscus [84]. The relationship between the wire diameter, and the equilibrium contact angle at the meniscus is defined by

$$\frac{h_m}{d_w} = 0.5 cos\varnothing_e \left(cosh^{-1}\frac{d_n}{d_w cos\varnothing_e} - cosh^{-1}\frac{1}{cos\varnothing_e} \right) \quad (13.4)$$

where h_m is the instantaneous height of the meniscus, d_w is the wire diameter, d_n is the nozzle diameter, and $\varnothing_e$ is the equilibrium contact angle. The wire diameter also scales as $d_w = k(I/v_n)^{1/2}$ where k is a proportionality constant, I is the ionic current, and v_n is the nozzle retraction speed. These relationships are found to be in good agreement with the experimental and modeling data [84].

4.4.2. Possible approaches to overcome resolution challenges in MCED

The resolution of the process is fundamentally limited by the nozzle diameter, applied ionic potential across the system, the nozzle retraction speed, and the thermodynamic stability of the three-phase meniscus. A smaller nozzle diameter, higher retraction velocity and reduced hydrophobicity of the substrate will yield higher resolution prints. However, from a practical standpoint, working with submicron nozzle sizes leads to nozzle clogging issues. Experimental results for deposition of wire bonds have shown that above a retraction speed ~270 nm/s, the liquid instabilities at the free surface often led to discontinuities in the meniscus, while very low retraction speeds (~100 nm/s) lead to nozzle clogging. Maintaining a uniform relative humidity in the print environment can potentially facilitate the stability of the nozzle [92]. Understanding the effect of the parameters on electrohydrodynamic computational models can help in optimizing the overall printing resolution without affecting the stability and throughput of the process [84, 92].

4.5. Throughput

4.5.1. Process throughput capabilities and challenges

The throughput of the electrodeposition processes is limited by the electroplating rate which is dependent on the applied overpotential and mass transport characteristics. Typical growth rates are limited to 100–500 nm/s for submicron parts [80,81,90]. At higher applied potentials, evolution of hydrogen ions can affect the process. The retraction velocity of the nozzle is limited by the growth rate of the structure, and is defined by [81,84].

$$v_n = -\frac{M_x I_x}{z_x \rho_x F} \quad (13.5)$$

where M_x is the molar mass, z_x, is the mobility of the charged species, ρ_x is the density of the bulk metal, I_x is the local current density (reaction kinetics are defined by the Butler-Volmer expression [93]) and, F is Faraday's constant. As the nozzle speed increases, the effective evaporation of water increases, and the meniscus is stretched (h_m increases). The radius of the meniscus and reduction of the ions at the growth front go down significantly [81,84]. This implies that the concentration of the ions within the meniscus increases. Evaporation also drives the flux of ions towards the meniscus surface. However, beyond a certain range of v_n, the ionic gradient between the growth front and nozzle exit leads to instabilities in the meniscus growth and stops the electrodeposition process. The deposition rate also increases with a decrease in nozzle diameter [84].

4.5.2. Possible approaches to overcome throughput challenges in MCED

The general rule of thumb for increasing the throughput of the electrodeposition process is to decrease the nozzle diameter and applied potential. Additionally, better control over the shape of the growth meniscus can help in avoiding nozzle clogging and discontinuities in the process. The electrodeposition process, however, will be primarily dependent on the kinetics of the electrochemical reactions. Like other DIW process, parallelizing the process with multiple nozzles might be useful in increasing the overall volumetric deposition throughput, but there are typical challenges associated with establishing very close menisci and introducing instabilities during the menisci growth.

4.6. Prognoses

Meniscus-confined electrodeposition process provides several advantages over traditional microscale AM processes by leveraging ionic gradient for fabricating highly dense microproducts. Several variants of the electrodeposition process are being developed to improve its geometric stability and explore a wider design space. The overall simplicity of the setup makes the process more conducive for mass production. Conversely, the fundamental nature of the electrodeposition process is also impeding its ability to undergo mass commercialization. It can process only conductive metals and the rate of electrochemical reactions severely affect the throughput of the process. These challenges can be primarily overcome by understanding the physical mechanisms associated with electrodeposition of different types of materials and the identifying the printing regimes within which the process is stable.

5. Laser-enabled electrochemical printing

5.1. General process of laser-enabled electrochemical printing (LECP)

Laser-enabled electrochemical printing (LECP) is a class of rapid prototyping technology that exploits electrochemical processes and a high speed laser to produce 2D films and 3D parts. As seen in Fig. 4a, in a typical LECP process, the laser-induced electrical field drives the transfer of charged particles, constrained at the liquid-solid or molecular-solid interfaces to form 2D films or 3D structures. LECP includes three major types: (1) laser-assisted electrophoretic deposition [94,99,100], (2) laser-enhanced electroplating deposition [97, 101–103], and (3) electrochemical photon-deposition [104–106]. LECP has a broad variety of material choices and has been used to print integrated electronics, sensors [94], and devices for photonics [95], energy [96], chemical, and biological applications [97]. In comparison with regular electrochemical deposition methods, LECP provides improved precision, a wider range of material choices, and the capability to fabricate arbitrary structures. LECP can directly print metals, semiconductors, nanoparticles, or polymer structures with a resolution of 0.1–10 μm. One limitation of the LECP process is that its throughput is limited by the sequential laser scanning process, where the focus of the laser drives the electrochemical processes for material deposition. Moreover, the higher the laser activation energy used, the slower the deposition rate will be. Higher throughput may be achieved by applying multiple laser beams for parallel scanning [98].

5.2. Materials

5.2.1. Capabilities and challenges of LECP

A wide range of materials (*e.g.,* metals, semiconductors, nanoparticles, nanocrystals, organics etc.) can be fabricated by LECP; however different materials systems and structures may require different system configurations and processing details. Conductive and photoactive materials have the right characteristics for the LECP process, but they are deposited using different mechanisms. For example, gold

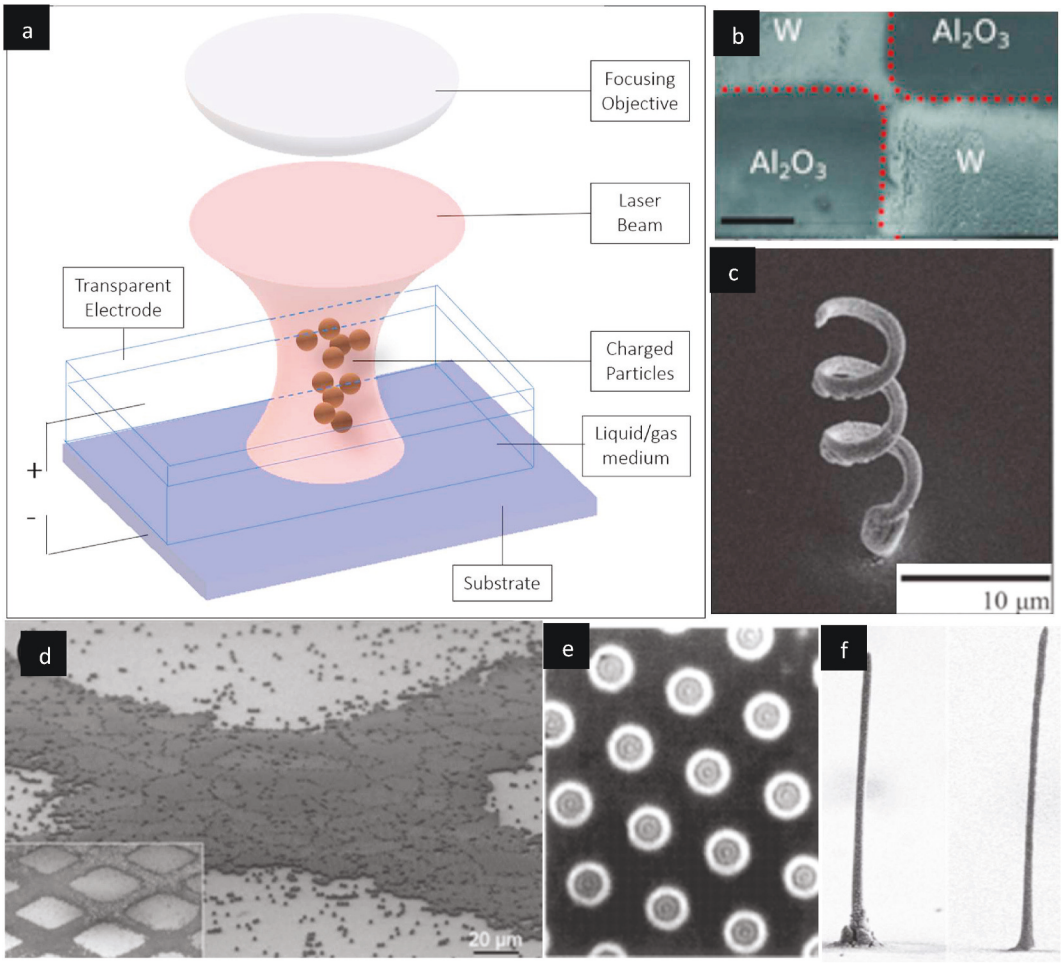

Fig. 4. a) Configuration of laser-enabled electrochemical printing (LECP) processes, which include an electrochemical system and a laser beam for selective deposition [90]. In this process, sequential and selective electrodeposition can be achieved by a laser. b) Scanning electron microscopy (SEM) image of a 2D tungsten composite pattern formed by light-directed electrophoretic deposition, the scale bar is 500 μm [111]. c) SEM image of a micro-helical spring made of gold nanoparticles [107]. d) SEM image of a patterned of colloid particles [100]. e) Image of palladium dots deposited from an aqueous solution, the average diameter the microsphere is ~6.6 μm [109]. f) SEM image of 3D LECP printed pillars of gold nanoparticles of different scales. The diameter of the left/right pillars are 2 μm/500 nm respectively [107]. (For interpretation of the references to colour in this figure legend, the reader is referred to the Web version of this article.)

nanoparticles can be deposited by spatial confinement via a laser focus on the surface of a target substrate, where an electrical voltage drives the deposition process [107]. CdTe nanocrystals can be deposited by appropriate laser irradiation that induces electric charges for deposition, *i.e.*, selective laser-induced electrophoretic deposition [95]. With a similar deposition mechanism, amorphous selenium colloidal material in solution (Fig. 4d) can be deposited on a substrate within tens of seconds [104]. Other metals, *e.g.*, tungsten (Fig. 4b), Mo, nickel [103, 108], gold [97], silver [101], protactinium [109], aluminum [106], and palladium [110](Fig. 4e), have been also reported to form depositions. Recently, ultrathin graphene has been fabricated by combining photolithography with the selective electrophoretic process [96].

In contrast to conductive materials, it is challenging to apply the LECP process to fabricate materials that are non-polar or photon insensitive. This is because in such materials, (1) it is difficult to generate electron-hole pairs using photon-enabled electronic transfer; and (2) the charge transfer reaction contributed by electrochemical potential is not enough to induce material deposition. It should be noted that both the solution chemistry and the choice of substrates are great importance for LECP.

5.2.2. Possible approaches to overcome material challenges in LECP

One possible way to address the LECP fabrication limitation for non-polar and photo-insensitive materials is to exploit the atom force microscopy (AFM) and focused ion beam (FIB) technologies that generate Van-der-Waals forces and strong discharge strengths respectively. Accordingly, transfer of charged particles may be induced using one of these mechanisms, which leads to controlled deposition. Notably, both AFM and FIB technologies can control the fabrication resolution at submicron scale at the expense of substantially reduced throughput and increased cost.

5.3. 3D fabrication

5.3.1. LECP for fabricating 3D structures

The LECP method is a high-precision selective process, which has been frequently used for generating high-resolution 2-D patterns of different materials and on various substrates. Complex 3D structures can also be fabricated via a layer-by-layer stacking LECP process; however, due to the limited throughput, the LECP 3D fabrication has only been used for process and laboratory demonstration purposes and lacks practical applications. 3D structures, such as pillars [107], coils [107] (Fig. 4c), walls [95,112] and overhanging structures [95], have been fabricated via light-assisted electrochemical printing methods. Furthermore, complex 3D microstructures made of gold nanoparticles have been successfully fabricated by manipulating the liquid cell via

laser trapping. Fig. 4f shows a nano-pillar with an average diameter of 500 nm[107]. A gold coil was fabricated by moving the liquid cell along a vortex trajectory while the gold particles are deposited [95]. A monolithic CdTe crystal was fabricated in a conformal layering process in which the electric field guides the growing direction [95]. Notably, as seen by Mora et al. [94], an enhanced light-directed electrophoretic deposition system was developed by using a projection-based system that not only eliminates a need for physical masks, but also allows the depositing pattern to change continuously, which resembles the projection stereolithography process. In a demonstration, an ultrathin graphene film with a thickness of 25 nm was rolled to form a 3D single-layer nanotube [96]. The LECP process and the recent development open a new route to the fabrication of complex and functional structures for scientific and engineering applications.

5.3.2. Possible approaches to overcome challenges in fabricating 3D structures

As mentioned, the bottleneck of the LECP process is its limited throughput. Most reported methods, however, are more suitable for 2-D surface patterning, coating, or physio-chemical modification than true 3D fabrication [108,112,113]. To enhance fabrication rate, one may apply multiple laser foci to parallelize the fabrication process; this may be achieved by using a micro-lens array, spatial light modulator, or a digital micromirror device (DMD) [98,114].

5.4. Feature size resolution

5.4.1. Capabilities and challenges of feature size resolution of LECP

The reported resolution of most LECP processes range from 0.1 to 10 μm[96,101,103,104,107,109]. The minimum feature size is highly dependent on the laser power, spot size, photon distribution (*i.e.*, point spread function), and wavelength. Generally, higher laser power increases the laser spot size and can trap more nanoparticles in the focus. This increases the fabrication rate at the expense of feature resolution, while low laser intensity will decrease the deposition rate with the benefit of improved resolution. Although in principle the fabrication resolution is limited by the optical diffraction limit, sub-diffraction features may be fabricated by precisely thresholding the laser power. Notably, this sub-wavelength fabrication may substantially compromise the throughput and uniformity of the fabricated structures and is difficult to achieve for large-area fabrication. To estimate the fabrication resolution, consider the nano-pillar in Fig. 4f, which has a diameter of 500 nm; this is equivalent to the size of the Airy disc, *i.e.*, $d = 1.22\lambda / NA = 496$ nm, where $\lambda = 488$ nm is the laser wavelength and $NA = 1.2$ is the numerical aperture. As such, the nano-pillar is diffraction limited. In other words, the minimum feature size depends on the laser spot size where trapped nanoparticles are confined [107]. Similar analyses can be performed in other experiments, for example, the diameter of the amorphous selenium composite was measured to be 0.5 μm which corresponds to the theoretical laser spot size of 488 nm[104]; the silver particle size was ~200 nm when irradiated under a 266 nm laser for laser plating [101]. Sub-diffraction fabrication has been demonstrated via a laser induced 3D deposition of CdTe nanocrystal in an aqueous solution, where a diameter of 500 nm was achieved, which is much smaller than the laser spot size [95]. The photon distribution of the laser beam will also influence the final feature size. For example, a Gaussian beam has a higher intensity in the center region; and a Bessel beam has a narrow and long photon distribution [108].

5.4.2. Possible approaches to overcome the current limits of feature resolution

The feature resolution depends on the laser power, spot size, photon distribution, and wavelength. In general, the feature resolution of LECP can be improved by improving spatially resolved control of the laser power, use of lasers with shorter wavelengths, or novel beam modes, *e.g.*, a Bessel beam may be used to improve the lateral resolution of 2D patterns. A beam homogenizer may be included in the current optical systems to improve the fabrication uniformity. In regard to photon distribution, a recently reported technique achieves sub-diffraction structures[262] by inducing and extending the lifetime of charged particles to ~10 s ms via an ultrafast laser.

5.5. Throughput

5.5.1. Capabilities and challenges of the throughput of LECP

The fabrication rate of the LECP process varies significantly with the material choices, processing conditions, and structure complexity. For example, Takai et al. [107] demonstrated that the LECP fabrication of gold nanoparticles has a throughput of $\sim 2.0 \times 10^{-4}$ mm^3/h. For amorphous selenium, the throughput is ~0.22 mm^3/h[104]. Silver particles have a throughput of $\sim 3.0 \times 10^{-3}$ mm^3/h[101], thin films of tungsten, molybdenum, nickel have a throughput of $\sim 7.2 \times 10^{-3}$ mm^3/h[103], and gold spot ~28 mm^3/h[97]. As can be seen, the throughput of LECP methods varies greatly depending on materials, dimensions and complexity of structures fabricated.

The LECP throughput is limited by several factors. Firstly, the throughput driven primarily by the growth rate of composites, which itself is dominated by the mass transport of nanoparticles into the focal spot of the trapping beam (*i.e.* the quality of the synthesized liquid solution). The deposition velocity can be sped up by increasing the concentration of the medium as well as by increasing laser power (and thus particle transfer) of the medium. However, there is a trade-off between the two. Increasing laser power will cause higher absorption, and the scattering of the laser beam will therefore prevent a significant increase in particle concentration. On the other hand, decreasing of the concentration of the medium will cause less particles to interact with the laser and thus drive fabrication throughput lower. Other parameters such as the surface activation energy and the laser scanning velocity can be controlled to achieve high throughput. The surface activation energy is very sensitive to temperature variation of the substrate. There has been evidence that high activation energy can cause reduced deposition throughput [109].

5.5.2. Possible approaches to overcome the current throughput limits in light-enabled electrochemical printing

Possible approaches to overcome the current throughput limits in light-enabled electrochemical printing are mainly focus on better control of activation energy, as the surface activation energy is essential to throughput of LECP methods. The substrate temperature depends on the thermal conductivity of the substrate and can be varied by controlling laser intensity. Lower laser intensity and higher thermal conductivity are preferred because it keeps the surface activation energy low without reducing throughput [109]. Controlling the wavelength of the laser can also influence the process. For example, both the absorption and Rayleigh scattering of gold solutions were significantly reduced within a wavelength of 500 nm and below. Another approach to control surface activation energy is to use a transparent substrate that can reduce the temperature increase of the substrate caused by the substrate absorption. The use of physical photomasks can compromise throughput. Recently, a solution to eliminate the physical mask was realized by using a digital projector to dynamically modify the illumination pattern in the light-direct electrophoretic deposition method [115]. Furthermore, high-speed scanning of the laser beam and using multi-beam configurations are other promising approaches worthy of investigation for high printing throughput in LECP [98].

5.6. Prognoses

LECP has the potential to transform the role of traditional electrochemical methods (*e.g.*, electrophoretic deposition and electroplating) from a deposition process to AM process for a wide variety of material choices. Recent advances in LECP processes have shed light on

simultaneously improving the resolution and rate by methods discussed in the previous sections.

6. Conclusions

This article in the third in the series of articles which investigate the state-of-the art in microscale additive manufacturing and the challenges and opportunities regarding their scalability. Energy-induced deposition and electrochemical approaches have demonstrated complex micro-fabrication capabilities with a variety of conductive materials. However, these processes are highly rate-dependent, due to the chemical kinetics of the processes. FIBID can theoretically achieve sub-10 nm layer thicknesses during the deposition process, and approaches using ion-projection lithography (IPL) have been shown to improve the throughput. Similarly, holographic beam splitting techniques can be implemented to further increase the throughput of LCVD. However, in these processes, deposition kinetics are dependent on mass transfer and diffusion of the available species and trying to increase the speed will always be limited by the rate at which local replenishment of these species can occur. Electrochemical processes like MCED and LECP are also limited by the rate at which mass transport of charged species occurs at the regions of applied potential. While the throughput of these processes can be somewhat improved by parallelizing them using multinozzle assemblies (in MCED) and spatial light modulators (in LECP), the rate of electroplating or electrophoretic deposition will still be limited by the materials being used. Considering the fundamental limits of the processes, general design guidelines for these processes have been explored in Part IV of the series of articles.

Contributions

SC, LS, RP, JH reviewed and wrote the section on LCVD. NR wrote the section on FIBID. XZ and SC wrote the section on LECP. DB and MC wrote the section on MCED and reviewed and edited the rest of the paper.

Declaration of competing interest

The authors declare that they have no known competing financial interests or personal relationships that could have appeared to influence the work reported in this paper.

Acknowledgements

This series of publications is a joint effort by the members and affiliates of the Micro-Nano Technical Leadership Committee of the American Society for Precision Engineering (ASPE). This work was supported in part by AFOSR under award number FA9550-18-1-0459 and by Prof. Hopkins' DOE-nominated Presidential Early Career Award for Scientists and Engineers under award number B620630. This work was performed under the auspices of the U.S. Department of Energy by Lawrence Livermore National Laboratory under Contract DE-AC52-07NA27344. LLNL-JRNL-807723.

References

[1] Behera D, Cullinan MA. Current challenges and potential directions towards precision microscale Additive manufacturing – Part I: direct ink writing/jetting processes. Precis Eng 2020.
[2] Behera D, et al. Current challenges and potential directions towards precision microscale Additive manufacturing – Part II: laser-based trapping, curing and heating processes. Precis Eng 2020.
[3] Behera D, et al. Current challenges and potential directions towards precision microscale Additive manufacturing – Part IV: future perspectives. Precis. Eng. Submitted 2020.
[4] Tseng AA. Recent developments in nanofabrication using focused ion beams. Small 2005;1:924–39.
[5] Chen P. Three-dimensional nanostructures fabricated by ion-beam-induced deposition. 2010.
[6] Tseng AA. Recent developments in micromilling using focused ion beam technology. J. micromechanics microengineering 2004;14:R15.
[7] Utke I, Hoffmann P, Melngailis J. Gas-assisted focused electron beam and ion beam processing and fabrication. J. Vac. Sci. Technol. B Microelectron. Nanom. Struct. 2008;26:1197.
[8] Kwakman L, et al. A comparison of Xenon plasma FIB technology with conventional gallium LMIS FIB: imaging, milling, and gas-assisted applications. Microsc Microanal 2011;17:652–3.
[9] Reyntjens S, Puers R. A review of focused ion beam applications in microsystem technology. J Micromech Microeng 2001;11:287–300.
[10] Reyntjens S, Puers R. Focused ion beam induced deposition: fabrication of three-dimensional microstructures and Young's modulus of the deposited material. J Micromech Microeng 2000;10:181.
[11] Peinado P, Sangiao S, De Teresa JM. Focused electron and ion beam induced deposition on flexible and transparent polycarbonate substrates. ACS Nano 2015;9:6139–46.
[12] Morita T, et al. Free-space-wiring fabrication in nano-space by focused-ion-beam chemical vapor deposition. J. Vac. Sci. Technol. B Microelectron. Nanom. Struct. 2003;21:2737.
[13] Esposito M, et al. Triple-helical nanowires by tomographic rotatory growth for chiral photonics. Nat Commun 2015;6:1–7.
[14] Gamo K, Takehara D, Hamamura Y, Tomita M, Namba S. Maskless ion beam assisted deposition of W and Ta films. Microelectron Eng 1986;5:163–70.
[15] Fujita J, et al. Structure and resonant characteristics of amorphous carbon pillars grown by focused-ion-beam-induced chemical vapor deposition. Jpn J Appl Phys 2002;41:4423.
[16] Telari KA, et al. Characterization of platinum films deposited by focused ion beam-assisted chemical vapor deposition. J. Vac. Sci. Technol. B Microelectron. Nanom. Struct. Process. Meas. Phenom. 2002;20:590–5.
[17] Ro JS, Thompson CV, Melngailis J. Mechanism of ion beam induced deposition of gold. J. Vac. Sci. Technol. B Microelectron. Nanom. Struct. Process. Meas. Phenom. 1994;12:73–7.
[18] Gross ME, Harriott LR, Opila RL. Focused ion beam stimulated deposition of aluminum from trialkylamine alanes. J Appl Phys 1990;68:4820–4.
[19] Della Ratta AD. Focused-ion beam induced deposition of copper. J. Vac. Sci. Technol. B Microelectron. Nanom. Struct. 1993;11:2195.
[20] Campbell AN, et al. Electrical and chemical characterization of FIB-deposited insulators. In: Proceedings of the 23rd international symposium for testing and failure analysis; 1997. p. 223–30. https://doi.org/10.2172/532558. ISTFA 1997.
[21] Edinger K. Study of precursor gases for focused ion beam insulator deposition. J. Vac. Sci. Technol. B Microelectron. Nanom. Struct. 1998;16:3311.
[22] Young RJ, Puretz J. Focused ion beam insulator deposition. J Vac Sci Technol B 1995;13:2576–9.
[23] Kometani R, et al. Performance of nanomanipulator fabricated on glass capillary by focused-ion-beam chemical vapor deposition. J. Vac. Sci. Technol. B Microelectron. Nanom. Struct. Process. Meas. Phenom. 2005;23:298–301.
[24] Igaki J ya, et al. Three-dimensional rotor fabrication by focused-ion-beam chemical-vapor-deposition. Microelectron Eng 2006;83:1221–4.
[25] Tasco V, et al. Three-dimensional nanohelices for chiral photonics. Appl Phys A Mater Sci Process 2016;122.
[26] Chen P, et al. Nanopillar growth by focused helium ion-beam-induced deposition. Nanotechnology 2010;21.
[27] Gerlach R, Utlaut M. Focused ion beam methods of nanofabrication: room at the bottom. Proc SPIE - Int Soc Opt Eng 2001;4510:96–106.
[28] Matsui S. Focused-ion-beam deposition for 3-D nanostructure fabrication. Nucl Instrum Methods Phys Res Sect B Beam Interact Mater Atoms 2007;257:758–64.
[29] Kometani R, et al. Nanomanipulator and actuator fabrication on glass capillary by focused-ion-beam-chemical vapor deposition. J. Vac. Sci. Technol. B Microelectron. Nanom. Struct. 2004;22:257.
[30] Kometani R, et al. Cell wall cutting tool and nano-net fabrication by FIB-CVD for subcellular operations and analysis. Microelectron Eng 2006;83:1642–5.
[31] Wanke MC, Lehmann O, Müller K, Wen Q, Stuke M. Laser rapid prototyping of photonic band-gap microstructures. Science 1997;275:1284–6.
[32] Xu Z, Kosugi T, Gamo K, Namba S. An x-ray photoelectron spectroscopy study on ion beam induced deposition of tungsten using tungsten hexafluoride. J Vac Sci Technol, B 1989;7:1959–62.
[33] Perentes A, Sinicco G, Boero G, Dwir B, Hoffmann P. Focused electron beam induced deposition of nickel. J. Vac. Sci. Technol. B Microelectron. Nanom. Struct. Process. Meas. Phenom. 2007;25:2228–32.
[34] Boden SA, Moktadir Z, Bagnall DM, Mizuta H, Rutt HN. Focused helium ion beam milling and deposition. Microelectron Eng 2011;88:2452–5.
[35] Matsui S, et al. Three-dimensional nanostructure fabrication by focused-ion-beam chemical vapor deposition. J. Vac. Sci. Technol. B Microelectron. Nanom. Struct. Process. Meas. Phenom. 2000;18:3181–4.
[36] Esposito M, et al. Tailoring chiro-optical effects by helical nanowire arrangement. Nanoscale 2015;7:18081–8.
[37] Puers R, Reyntjens S. Fabrication and testing of custom vacuum encapsulations deposited by focused ion beam direct-write CVD. Sensors Actuators, A Phys. 2001;92:249–56.
[38] DeMarco AJ, Melngailis J. Lateral growth of focused ion beam deposited platinum for stencil mask repair. J. Vac. Sci. Technol. B Microelectron. Nanom. Struct. 2002;17:3154.
[39] Kim H-B, Hobler G, Lugstein A, Bertagnolli E. Simulation of ion beam induced micro/nano fabrication. J Micromech Microeng 2007;17:1178.

[40] Nagel DJ. Technologies for micrometer and nanometer pattern and material transfer. Direct-Write Technologies for Rapid Prototyping 2002:557–679. https://doi.org/10.1016/B978-012174231-7/50072-5.
[41] Rahman FHM, et al. The prospects of a subnanometer focused neon ion beam. Scanning 2012;34:129–34.
[42] Ward BW, Notte JA, Economou NP. Helium ion microscope: a new tool for nanoscale microscopy and metrology. J. Vac. Sci. Technol. B Microelectron. Nanom. Struct. 2006;24:2871.
[43] Cohen-Tanugi D, Yao N. Superior imaging resolution in scanning helium-ion microscopy: a look at beam-sample interactions. J Appl Phys 2008;104:63504.
[44] Wu H, et al. Focused helium ion beam deposited low resistivity cobalt metal lines with 10 nm resolution: implications for advanced circuit editing. J Mater Sci Mater Electron 2014;25:587–95.
[45] Alkemade PFA, Miro H. Focused helium-ion-beam-induced deposition. Appl Phys A 2014;117:1727–47.
[46] Hon KKB, Li L, Hutchings IM. Direct writing technology-Advances and developments. CIRP Ann - Manuf Technol 2008;57:601–20.
[47] Melngailis J. A review of ion projection lithography. J. Vac. Sci. Technol. B Microelectron. Nanom. Struct. 2002;16:927.
[48] Ampere AT. Recent developments in nanofabrication using ion projection lithography. Small 2005;1:594–608.
[49] Platzgummer E, et al. Charged particle multi-beam lithography evaluations for sub-16nm hp mask node fabrication and wafer direct write. Photomask Technology 2009;7488. 74881D (2009).
[50] Letzkus F, et al. Deflection unit for multi-beam mask making. In: 25th European mask and lithography conference, vols. 1–12; 2009.
[51] Matsumoto H, Yamashita H, Tamura T, Ohtoshi K. Multi-beam mask writer MBM-1000. In: Photomask Japan 2017: XXIV symposium on photomask and next-generation lithography mask technology, vol. 10454; 2017, 104540E.
[52] Tseng AA, Tanaka M. Advanced deposition techniques for freeform fabrication of metal and ceramic parts. Rapid Prototyp J 2001;7:6–17.
[53] Hahmann P, et al. High resolution variable-shaped beam direct write. Microelectron Eng 2007;84:774–8.
[54] Caricato AP, Kudryavsev YV, Luches A, Mulenko SA. In: Dumitras DC, Dinescu M, Konov VI, editors. Deposition of semiconductor thin films with narrow band gap based on iron oxides by using laser radiation (LCVD and RPLD). vol. 6606. International Society for Optics and Photonics; 2007. 66060T-66060T–11.
[55] Stuke M, et al. Laser-direct-write creation of three-dimensional OREST microcages for contact-free trapping, handling and transfer of small polarizable neutral objects in solution. Appl Phys A 2005;81:915–22.
[56] Maxwell JL, et al. High-speed laser chemical vapor deposition of amorphous carbon fibers, stacked conductive coils, and folded helical springs. In: Symposium on micromachining and microfabrication; 1999. p. 227–35. https://doi.org/10.1117/12.361225.
[57] Vaezi M, Seitz H, Yang S. A review on 3D micro-additive manufacturing technologies. Int J Adv Manuf Technol 2013;67:1721–54.
[58] Heszler P, Landstrom L. Laser-induced nanoparticle formation. In: Vajtai R, Aymerich X, Kish LB, Rubio A, editors. SPIE 5118, nanotechnology; 2003. p. 60. https://doi.org/10.1117/12.498569.
[59] Allen SD. Laser chemical vapor deposition-applications in materials processing. 0198. In: Ready JF, editor. Laser applications in materials processing, vols. 49–56. International Society for Optics and Photonics; 1980.
[60] Tang M, Zhang H, McCoy J, Her T-H. Periodic nanoripple generated by femtosecond laser beam in LCVD system. In: Maher M-A, et al., editors. Proc. Of SPIE, vol. 6462; 2007. 64620T.
[61] Duty C, Jean D, Lackey WJ. Laser chemical vapour deposition: materials, modelling, and process control. Int Mater Rev 2001;46:271–87.
[62] Guss GM, Sridharan AK, Elhadj S, Johnson M a, Matthews MJ. Nanoscale surface tracking of laser material processing using phase shifting diffraction interferometry. Optic Express 2014;22:14493.
[63] Mahjouri M, Zhou YS, Xiong W, Lu YF. Growth of self-aligned single-walled carbon nanotubes by laser-assisted chemical vapor deposition. In: Pfleging W, Lu Y, Washio K, Hoving W, Amako J, editors. Proc. Of SPIE, vol. 6880; 2008, 68800P.
[64] Arnold N, Thor E, Kirichenko N, Bäuerle D. Pyrolytic LCVD of fibers: a theoretical description. Appl Phys A Mater Sci Process 1996;62:503–8.
[65] Mazumder J, Kar A. Photolytic LCVD. In: Theory and application of laser chemical vapor deposition. Springer US; 1995. p. 123–214. https://doi.org/10.1007/978-1-4899-1430-9_3.
[66] Allen SD. Laser chemical vapor deposition: a technique for selective area deposition. J Appl Phys 1981;52:6501–5.
[67] Pauleau Y, Tonneau D. Reaction mechanisms in laser-assisted chemical vapor deposition of microstructures. In: Chemical physics of thin film deposition processes for micro- and nano-technologies. Springer Netherlands; 2002. p. 223–54. https://doi.org/10.1007/978-94-010-0353-7_10.
[68] Duneau M, Delyon F, Audier M. Holographic method for a direct growth of three-dimensional photonic crystals by chemical vapor deposition. J Appl Phys 2004;96:2428–36.
[69] Lehmann O, Stuke M. Three-dimensional laser direct writing of electrically conducting and isolating microstructures. Mater Lett 1994;21:131–6.
[70] Banal R, Kimura T, Goto T. High speed deposition of Y 2 O 3 films by laser-assisted chemical vapor deposition 2005;46:2114–6.
[71] Lehmann O, Stuke M. Laser-driven movement of three-dimensional microstructures generated by laser rapid prototyping. Science 1995;270:1644–6.
[72] Lehmann O, Stuke M. Generation of three-dimensional free-standing metal micro-objects by Laser Chemical processing. Appl. Phys. A Solids Surfaces 1991;53:343–5.
[73] Capodieci L. From optical proximity correction to lithography-driven physical design (1996-2006): 10 years of resolution enhancement technology and the roadmap enablers for the next decade. In: SPIE 31st international symposium on advanced lithography - optical microlithography XIX, vol. 6154; 2006, 615401.
[74] Roy NK, et al. A comprehensive study of the sintering of copper nanoparticles using femtosecond, nanosecond, and continuous wave lasers. J Micro Nano-Manufacturing 2017;6. 010903.
[75] Maruo S, Nakamura O, Kawata S. Three-dimensional microfabrication with two-photon-absorbed photopolymerization. Opt Lett 1997;22:132.
[76] Malinauskas M, Žukauskas A, Bičkauskaitė G, Gadonas R, Juodkazis S. Mechanisms of three-dimensional structuring of photo-polymers by tightly focussed femtosecond laser pulses. Optic Express 2010;18:10209.
[77] Fischer J, et al. Three-dimensional multi-photon direct laser writing with variable repetition rate. Optic Express 2013;21:26244–60.
[78] Williams K, Maxwell J, Larsson K, Boman M. Freeform fabrication of functional microsolenoids, electromagnets and helical springs using high-pressure laser chemical vapor deposition. In: Technical digest. IEEE international MEMS 99 conference. Twelfth IEEE international conference on micro electro mechanical systems (cat. No.99CH36291). IEEE; 1999. p. 232–7. https://doi.org/10.1109/MEMSYS.1999.746821.
[79] Williams KL, Köhler J, Boman M. Fabrication and mechanical characterization of LCVD-deposited carbon micro-springs. Sensors Actuators A Phys 2006;130–131:358–64.
[80] Suryavanshi AP, Yu M. Probe-based electrochemical fabrication of freestanding Cu nanowire array. Appl Phys Lett 2006;88:8–10.
[81] Hu J, Yu M. Meniscus-confined three-dimensional electrodeposition for direct writing of wire bonds published by : American association for the advancement of science linked references are available on JSTOR for this article : meniscus-confined three-dimensional elect. Science 2010;329:313–6.
[82] Hirt L, et al. Template-free 3D microprinting of metals using a force-controlled nanopipette for layer-by-layer electrodeposition. Adv Mater 2016;28:2311–5.
[83] Suryavanshi AP. Meniscus controlled three-dimensional nanofabrication. University of Illinois at Urbana-Champaign; 2007.
[84] Morsali S, et al. Multi-physics simulation of metal printing at micro/nanoscale using meniscus-confined electrodeposition: effect of nozzle speed and diameter. J Appl Phys 2017;121.
[85] Suryavanshi AP, Yu MF. Electrochemical fountain pen nanofabrication of vertically grown platinum nanowires. Nanotechnology 2007;18.
[86] Seol SK, et al. Electrodeposition-based 3D printing of metallic microarchitectures with controlled internal structures. Small 2015;11:3896–902.
[87] Iwata F, Sumiya Y, Sasaki A. Nanometer-scale metal plating using a scanning shear-force microscope with an electrolyte-filled micropipette probe. Japanese J. Appl. Physics, Part 1 Regul. Pap. Short Notes Rev. Pap. 2004;43:4482–5.
[88] McKelvey K, O'Connell MA, Unwin PR. Meniscus confined fabrication of multidimensional conducting polymer nanostructures with scanning electrochemical cell microscopy (SECCM). Chem Commun 2013;49:2986–8.
[89] Kim JT, et al. Three-dimensional writing of conducting polymer nanowire arrays by meniscus-guided polymerization. Adv Mater 2011;23:1968–70.
[90] Hirt L, Reiser A, Spolenak R, Zambelli T. Additive manufacturing of metal structures at the micrometer scale. Adv Mater 2017;29.
[91] Momotenko D, Page A, Adobes-Vidal M, Unwin PR. Write-read 3D patterning with a dual-channel nanopipette. ACS Nano 2016;10:8871–8.
[92] Morsali S, et al. Multi-physics simulation of metal printing at micro/nanoscale using meniscus-confined electrodeposition: effect of environmental humidity. J Appl Phys 2017;121.
[93] Sokirko AV, Barks FH. Diffusion-migration transport in a system with butler-volmer kinetics, an exact solution. Electrochim Acta 1995;40:1983–95.
[94] Mora J, et al. Projection based light-directed electrophoretic deposition for additive manufacturing. Addit. Manuf. 2018;22:330–3.
[95] Shou W, Pan H. Direct printing of microstructures by femtosecond laser excitation of nanocrystals in solution. Appl Phys Lett 2016;108.
[96] Niu Z, et al. All-solid-state flexible ultrathin micro-supercapacitors based on graphene. Adv Mater 2013;25:4035–42.
[97] von Gutfeld RJ, Gelchinski MH, Romankiw LT, R V D. Laser-enhanced jet plating: a method of high-speed maskless patterning. Appl Phys Lett 1983;43:876–8.
[98] Geng Q, Gu C, Cheng J, Chen S. Digital micromirror device-based two-photon microscopy for three-dimensional and random-access imaging. Optica 2017;4:674.
[99] Takai T, Nakao H, Iwata F. Three-dimensional microfabrication using local electrophoresis deposition and a laser trapping technique. Opt Express 2014;22:2656–8.
[100] Hayward RC, A S D, A A I. Electrophoretic assembly of colloidal crystals with optically tunable micropatterns. Nature 2000;404:56–9.
[101] Chen D, Lu Q, Zhao Y. Laser-induced site-selective silver seeding on polyimide for electroless copper plating. Appl Surf Sci 2006;253:1573–80.
[102] Puippe JC, Acosta RE, Gutfeld R J von. Investigation of laser-enhanced electroplating mechanisms. J Electrochem Soc 2006;128:2539.
[103] Gutfeld R J von, Tynan EE, Melcher RL, Blum SE. Laser enhanced electroplating and maskless pattern generation. Appl Phys Lett 1979;35:651–3.
[104] Baal-Zedaka I, et al. Photodeposition of optical elements from colloid solutions. Colloids Surfaces A Physicochem. Eng. Asp. 2003;217:191–202.
[105] Kikuchi T, Chu SZ, Jonishi S, Sakairi M, Takahashi H. Local surface modification of aluminum by laser irradiation. Electrochim Acta 2001;47:225–34.

[106] Takahashi H, Sakairi M, Kikuchi T. Micro- and nano-technologies based on anodizing of aluminum – combination of laser irradiation with electrochemical process. Electrochemistry 2009;77:30–42.
[107] Takai T, Nakao H, Iwata F. Three-dimensional microfabrication using local electrophoresis deposition and a laser trapping technique. Optic Express 2014;22:28109.
[108] Jansson A, Thornell G, Johansson S. High resolution 3D microstructures made by localized electrodeposition of nickel. J Electrochem Soc 2002;147:1810.
[109] Bauerle D, Landstrom L, Kofler J, Arnold N, Piglmayer K. Laser processing with colloid monolayers. Phot. Process. Microelectron. Photonics III 2004;5339:20.
[110] Bauerle D, et al. Laser cleaning and surface modifications: applications in nano- and biotechnology. Laser Clean. II 2007. https://doi.org/10.1142/9789812706843_0001.
[111] Pascall AJ, et al. Light-directed electrophoretic deposition: a new additive manufacturing technique for arbitrarily patterned 3D composites. Adv Mater 2014;26:2252–6.
[112] Pan Y, Patil A, Guo P, Zhou C. A novel projection based electro-stereolithography (PES) process for production of 3D polymer-particle composite objects. Rapid Prototyp J 2017;23:236–45.
[113] Bäuerle D. Laser chemical processing: an overview to the 30th anniversary. Appl Phys A Mater Sci Process 2010;101:447–59.
[114] Geng Q, Wang D, Chen P, Chen SC. Ultrafast multi-focus 3-D nano-fabrication based on two-photon polymerization. Nat Commun 2019;10:1–7.
[115] Roy S. Fabrication of micro- and nano-structured materials using mask-less processes. J Phys D Appl Phys 2007;40.